Available online at www.sciencedirect.com
ScienceDirect
Ceramics International 37 (2011) 2845–2853
CERAMICS INTERNATIONAL
www.elsevier.com/locate/ceramint

Preparation of humidity-controlling porous ceramics from volcanic ash and waste glass

Dinh-Hieu Vu [a,b,*], Kuen-Sheng Wang [a], Bui Xuan Nam [b], Bui Hoang Bac [c], Tien-Chun Chu [a]

[a] Graduate Institute of Environmental Engineering, National Central University, No.300, Jhongda Rd., Jhongli, Taoyuan 32001, Taiwan
[b] Faculty of Mining, Hanoi University of Mining and Geology, Tu Liem, Hanoi, Viet Nam
[c] Faculty of Geology, Hanoi University of Mining and Geology, Tu Liem, Hanoi, Viet Nam

Received 14 January 2011; received in revised form 26 April 2011; accepted 28 April 2011
Available online 5 May 2011

Abstract

This work investigated the preparation of a humidity-controlling porous ceramic via sintering of a mixture of volcanic ash soil and waste glass at 800–815 °C for 5–10 min. The final products were analyzed to identify the porous and mechanical properties, the moisture adsorption–desorption performance characteristics, and the adsorbed moisture amount. The most superior ceramic product, manufactured by mixing 30% weathered volcanic ash and 70% waste glass, was sintered at 800 °C for 5 min. The porous properties included a BET surface area of 163.73 ± 12 m^2/g, porosity of 52.08 ± 2.1%, and a pore size of approximately 9 nm in diameter. The total amount of water adsorbed by the superior ceramic product was 0.047 cm^3/g. In addition, the mechanical characteristics, including a bulk density of 1.34 ± 0.2 g/cm^3, 2.61 ± 0.1% shrinkage, 4.64 ± 0.3% ignition loss, and 6.58 ± 0.4 MPa bending strength, are consistent with those of commercial porous ceramics. The leaching concentration of heavy metals in the final products were all well below the TCLP regulation limits. Thus, the most superior products meet the standards for commercial porous ceramics.

Keywords: Volcanic ash; Waste glass; Sintering; Mesoporous ceramic

1. Introduction

In residential construction technology, humidity and ventilation control are essential, and they must be considered during construction to prevent the building walls from retaining moisture and growing mold [1]. To control the environmental humidity in houses, various solutions have been employed, such as the use of air-conditioning or pressed organic materials in the walls [2–4]. However, these solutions have disadvantages; the use of air-conditioning for long periods of time is costly while the organic material used in the walls is flammable, weak, and non-durable. In some cases, inorganic compounds, such as calcium chloride, silica-gel, and clay-sand, have also been used as wall materials for [5–7], but these materials exhibit poor water adsorption-desorption ability, and are potentially harmful to human health [8]. Therefore, the development of a low-cost, energy-efficient and safe ceramic that incorporates inorganic materials for humidity control is desirable.

Certain porous materials, such as diatomaceous earth, sepiolite, silica gel, zeolite, and alumina gel, possess pore properties that are able to carry out capillary condensation. Recently, these materials have been recently used to control humidity and reduce energy consumption [9–14]. These mesoporous materials usually have a high specific surface area, significant porosity, and an appropriate pore structure, which enhance their ability to control the humidity in the environment. The relationship between the porous structure of a material and the capillary condensation mechanism is illustrated by the Kelvin equation:

$$\ln\left(\frac{P}{P_0}\right) = \frac{-2\gamma V_L}{RT}\frac{1}{r_c}$$

where, P/P_0 is the relative pressure of vapor in equilibrium with a meniscus having a radius of curvature r_c, γ and V_L are the

* Corresponding author at: Postal address: Graduate Institute of Environmental Engineering, National Central University, No. 300, Jhongda Rd., Jhongli, Taoyuan 32001, Taiwan. Tel.: +886 3 422 7151x34666; fax: +886 3 422 1602.
E-mail address: vudinhhieu@gmail.com (D.-H. Vu).

0272-8842/$36.00
doi:10.1016/j.ceramint.2011.04.118

surface tension and liquid molar volume of liquid adsorption, respectively. R is the gas constant, and T is the absolute temperature [15]. To form the sorption isotherm of a material, the material is placed in an environment where both the temperature and the humidity are appropriately controlled. The equilibrium moisture content is measured at each value of the ambient relative humidity. In addition, the adsorption behavior is limited by the capillary condensation mechanism, and at a specific level of humidity, the equilibrium absorption ability is proportioned to the accumulative pore volume with a diameter smaller than that determined by Kelvin's equation. Thus, to manufacture good porous mechanical ceramics that can control humidity, the pore size of the raw materials should be in the appropriate range of mesopore.

Weathered volcanic ash soil is quite common in the areas that have volcano activities. The main component of the weathered volcanic ash soil is allophane. This material has many specific properties, and it recently been of interest by many researchers [16–22]. The molecular structure of allophane contains chain-rings of linked silicate and tetrahedral or octahedral aluminates (four or eight oxygen atoms arranged at the points of a triangular pyramid or parallelepiped around a central silicon or aluminum atom) [18]. The diameter of the structure is in the range of 3.5 nm to 5 nm [19]. In addition, the structure has a low bulk density of 0.5 g/cm^3 [20] and large specific surface area of 2210 m^2/g [19]. With specific properties, allophane can be used to produce porous ceramics that are low-cost with well-defined porosity, low density, and high thermal stability.

Therefore, the objective of this paper is to study the ability of using natural porous materials (weathered volcanic ash soil), which have a large proportion of mesopores and which are abundant in deposit, mixed with waste glass to produce new porous ceramics that can control environmental humidity. Different sintering conditions and characteristics of the new ceramics will be studied.

2. Experimental

The materials, including weathered volcanic ash and waste glass, were collected from a material supplier in Taipei City (Taiwan). The materials were dried at 105 °C for 24 h and were then ground using a wet ball-mill machine for 24 h. The materials were then dried again at 105 °C. The powders were then passed through 0.075 mm sieves and were carefully stored in desiccators for subsequent experiments. The fine powders of waste glass and weathered volcanic ash were mixed together at various ratios (Table 1) to obtain a mixed powder: waste glass – weathered volcanic ash (GA). The mixed powders were then pressed uniaxially at 32 MPa and were molded into a green compact of 50 mm in diameter and 6 mm in height. The green compacts were dried at 100 °C and were then sintered in the electric-heated furnace at 800 °C and 815 °C for 5 to 10 min, respectively. All of the samples before analyses were dried at 105 °C for 24 h and were stored in desiccators.

Table 1
The ratios of waste glass and volcanic ash in the mixed powders (wt%).

Green samples (GA)	Waste glass	Weathered volcanic ash
G60A40	60	40
G70A30	70	30
G80A20	80	20

The characteristics of the initial materials and the products were determined by using various techniques. The chemical analysis was performed using the ICP-AES. The XRD pattern was recorded using an X'Pert PRO. The particle size distribution of the raw material were determined using a laser particle size analyzer (Rise-2006) with PEG-10000 (polyethylene glycol; molecular weight: 10,000 g mol^{-1}) as an organic dispersing agent. Nitrogen isotherms were determined using an ASAP 2010 Machine to analyze the pore size distribution. The surface area was measured using the BET method. The moisture isotherm and equilibrium moisture content of final products were determined at 23 °C by using a TEREHY-HRT-80FA Machine and the ASTM-1498-01 method [23]. Prior to testing the moisture adsorption, each test specimen was dried to a constant mass. The RH values were achieved either in the climatic chamber and were controlled to increase from the lowest values (10% RH) to the highest values (98% RH). For each RH value, the constant mass is reached if in five successive weightings, with 24 h intervals, the change of mass is less than 0.1% of the specimen mass, until the equilibrium is reached at each RH. The full sorption curve is completed when eleven values (RH) are selected. For the desorption process, the fully saturated specimen in a weighing cup was placed at the highest RH (98%RH). The whole procedure as described in the adsorption process was repeated until the measurement was completed at the lowest RH. The equilibrium moisture content at each RH value was calculated from the measured difference between the constant saturated mass and the dry weight of the specimen. The calculation of the moisture content, v (g g^{-1}), using the mean values of the mass of the test specimens at each RH: $v = (m - m_0)/m_0$; where, m is the mean mass of the specimens at equilibrium, and m_0 is the mean mass of the dry specimens.In addition, the bending strength was measured with a Twin Column Testing Machine (LR5KPlus) using the ASTM C1674-08 method [24] on 3 test pieces for each body by a three-point loading test with a span of 24 mm and a crosshead speed of 0.1 mm/min. Losses on the ignition of the final products were determined in accordance with the procedures outlined in test methods ASTM D7348-08 [25]. The calculation of the Ignition Loss was as follows, % = (A/B) × 100, where A is weight loss at sintering temperature, and B is weight of moisture fire sample used. The bulk density of the specimens was determined by Archimedes's immersion technique; the specimens were kept in boiling water for 3 h according to the ASTM C20-00(2010) method [26]. The geometry (diameter and thickness) of the sintered products was measured using a digital caliper to determine the apparent volume of the sintered product, V_T. The volume shrinkage can be calculated using the equation: $v = [(V_0–V_T)/V_T] \times 100\%$, where v is the volume shrinkage, V_0 is the volume of the green sample and V_T is the apparent volume of the sintered product.

Table 2
Chemical compositions of the raw materials (wt%).

Materials	SiO_2	Al_2O_3	Na_2O	K_2O	MgO	CaO	TiO_2	Fe_2O_3	ZrO_2	MnO	P_2O_5	Sum
Waste glass	66.44	1.63	14.29	0.96	0.52	10.71	0.02	0.09	0.07	0.23	0.34	95.3
Volcanic ash	47.01	19.48	1.58	0.77	0.35	2.31	0.19	1.90	0.60	0.11	0.15	74.45

Note: 4.7 wt% and 25.55 wt% are the H_2O components in waste glass and volcanic ash soil, respectively.

3. Results and discussion

3.1. Characteristics of the initial materials

Chemical analysis of the initial materials (Table 2) indicates that the main chemical components are SiO_2 (47.01%) and Al_2O_3 (19.48%) in the weathered volcanic ash soil and SiO_2 (66.44%) in the waste glass. In addition, there are small amounts of oxides of K, Mg, Ca, Ti, Fe, and so forth in both the volcanic ash soil and the waste glass. These results confirm that both volcanic ash and waste glass contain metallic iron, which can be used as a source material for producing ceramic. The XRD pattern of weathered volcanic ash soil shows two strong, broad reflections at 3.42 Å and 2.25 Å (Fig. 1A). These features indicate that allophane is the main component in weathered volcanic soil. This interpretation is similar to that of Lindner [19] and Opiso [22]. The XRD pattern of waste glass shows a large hump between 20° and 35° of 2θ, indicating the presence of a large number of amorphous phases in the sample (Fig. 1B), which is consistent with the findings of Das [27] and Tulyaganov [28]. These results indicate that weathered volcanic ash soil is a potential natural porous material for preparing porous ceramics in which waste glass is an adhesive agent. It is believed that the mixture of these materials would create new ceramics that have interesting porous properties.

The particle size distribution in the raw materials is shown in Fig. 2. The particle size distribution of the weathered volcanic ash exhibits a high peak at a particle size of 6 μm, and 90 wt% of the particles range in size from 2 to 15 μm. The waste glass particle size distribution exhibits a high peak at a particle size of 25 μm, and 90 wt% of the waste glass particles are less than 30 μm in size. Significantly, the particle sizes of the raw materials are homogenous; the homogeneity of the mixture is of prime importance to improve not only mechanical milling but also chemical processing, i.e., pore formation and co-precipitation processes, of the ceramic products. These findings further support the proposal of S.J. Kang [29]. The densities of the volcanic ash and waste glass are 0.55 ± 0.05 g/cm^3 and 2.31 ± 0.2 g/cm^3, respectively, while the porosities of the volcanic ash and waste glass are $75 \pm 3\%$ and $20 \pm 1\%$, respectively.

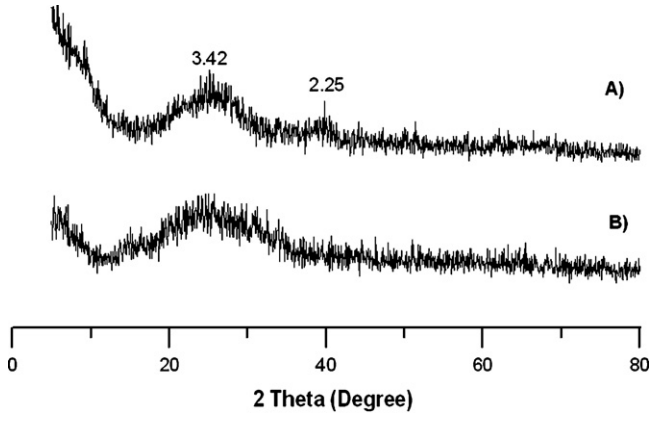

Fig. 1. XRD patterns of the weathered volcanic ash (A) and the waste glass (B). *(Number units: Angstroms).*

3.2. Characteristics of the porous ceramics

3.2.1. Porous properties

Nitrogen adsorption-desorption isotherms of the final ceramic products at sintering temperatures of 800 °C and 815 °C for 5–10 min are shown in Fig. 3. On the basis of the IUPAC classification system, all of the isotherms display Type IV behavior that is characteristic of mesopores present in the structures of these products [15]. In addition, the results of pore size analyses conducted using nitrogen adsorption measurements confirm that the pore sizes of all of the ceramics are distributed mainly in the range of 7–10 nm under the experimental conditions at 800 °C and 815 °C (Fig. 4). The BET surface areas and the porosity data for these mesoporous ceramics are summarized in Table 3. The BET surface areas range from 22.21 ± 3.0 to 418.88 ± 15 m^2/g, and the porosity ranges from 29.91 ± 1.5 to $54.53 \pm 1.6\%$. These data tend to gradually decrease as the sintering temperature increases from 800 °C to 815 °C. These data also decrease as the amount of waste glass in ratio of the raw materials increases. The effects of

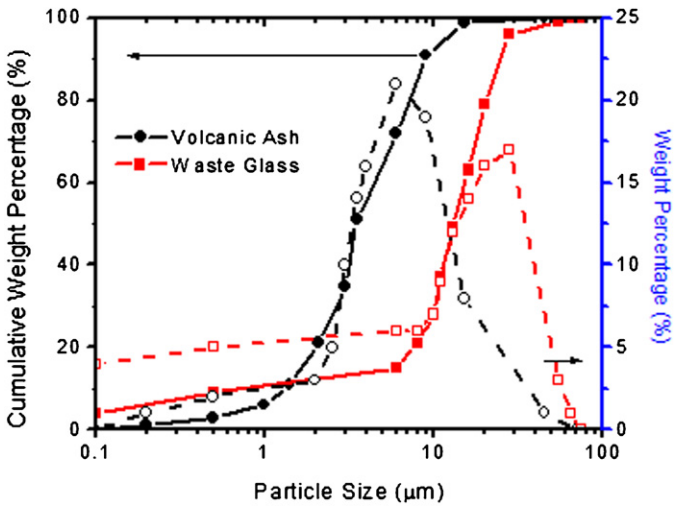

Fig. 2. Particle size distribution in the raw materials.

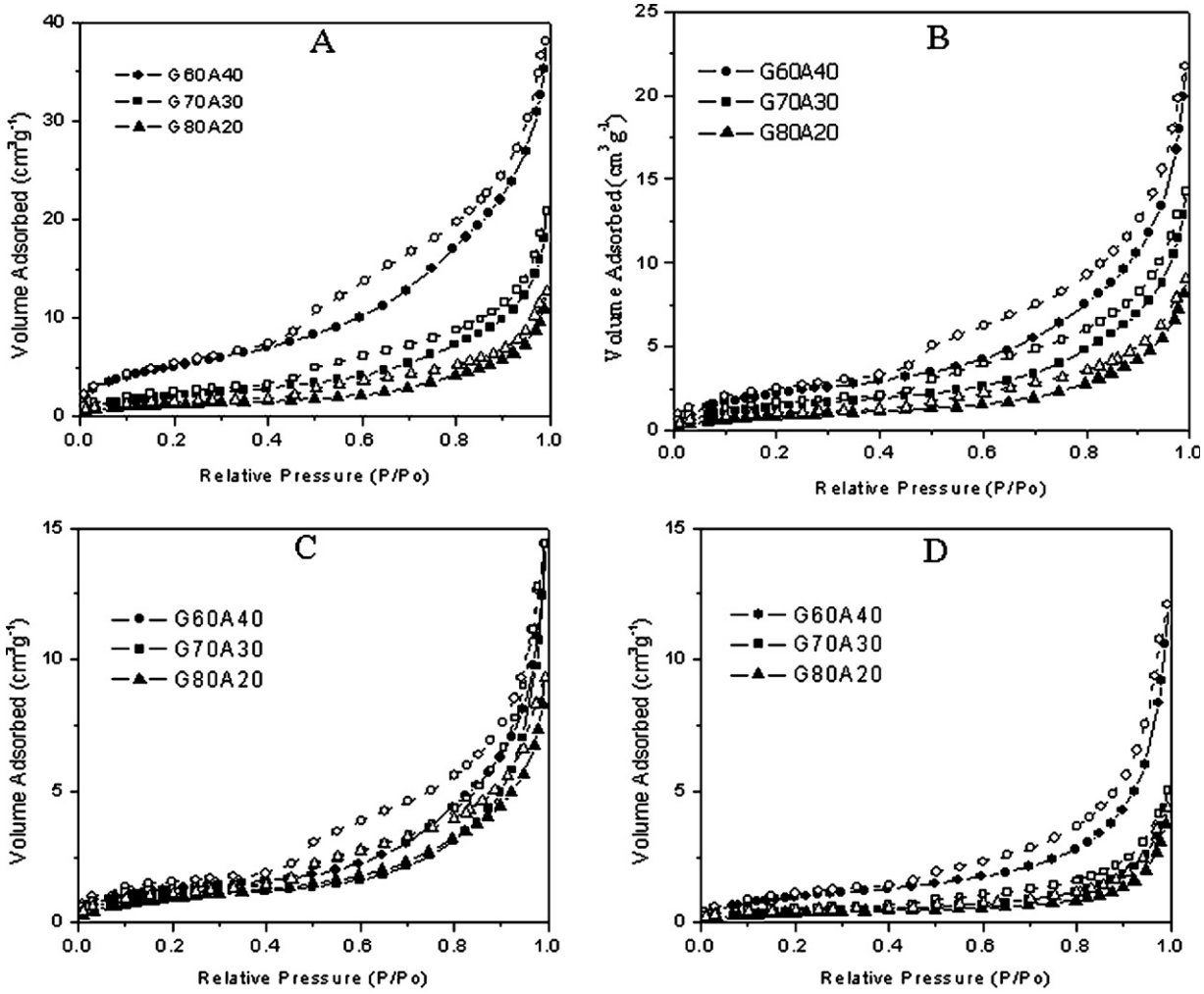

Fig. 3. Nitrogen isotherms of the final ceramic products sintered at 800 °C for 5 min (A), 800 °C for 10 min (B), 815 °C for 5 min (C), and 815 °C for 10 min (D). (*Filled symbols: adsorption; empty symbols: desorption*).

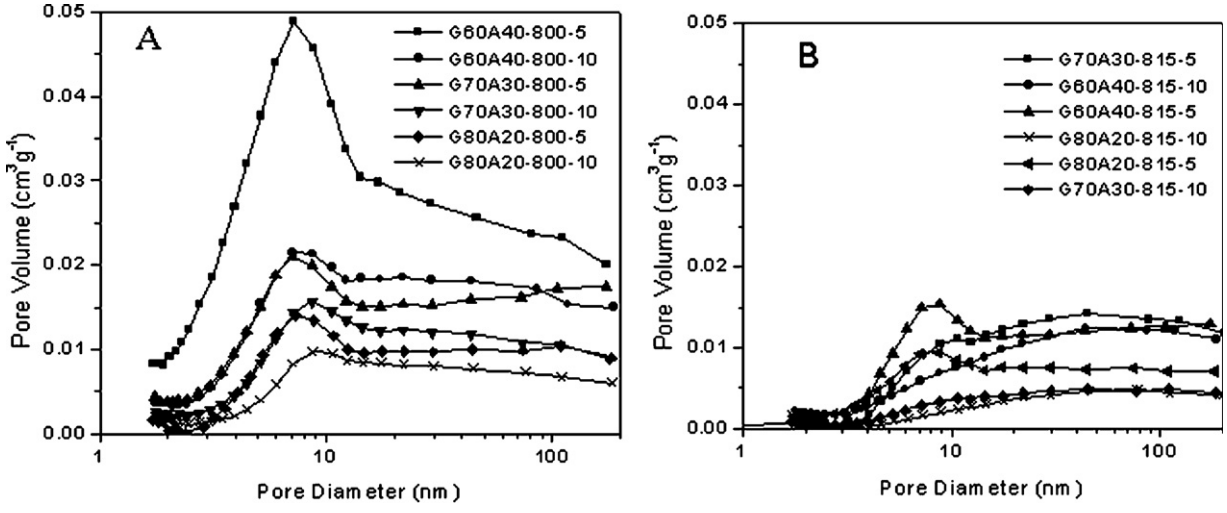

Fig. 4. Pore size distribution in the final ceramic products sintered at 800 °C (A) and 815 °C (B).

sintering temperature and time on the pore diameters present in the final products were also examined by SEM analysis. Fig. 5 shows SEM images of the representative G70A30 product at different temperatures and holding times. The observed porosity of these materials may be explained by sintering theory [29]. According to this theory, the densification and subsequent shrinkage of a compacted powder are achieved by the transport of material from the contact area between grains

Table 3
Porous and mechanical properties of the final ceramic products.

Sintering temp./time (°C/min)	Samples	Porous properties		Mechanical properties			
		BET Surface Area (m^2/g)	Porosity (%)	Bulk Density (g/cm^3)	Bending strength (MPa)	Shrinkage (%)	Ignition loss (%)
800/05	G60A40	418.88 ± 15	54.53 ± 1.6	1.27 ± 0.3	5.56 ± 0.5	2.43 ± 0.2	5.44 ± 0.5
	G70A30	163.73 ± 12	52.08 ± 2.1	1.34 ± 0.2	6.58 ± 0.4	2.61 ± 0.1	4.64 ± 0.3
	G80A20	76.89 ± 9	51.65 ± 2.3	1.39 ± 0.3	6.68 ± 0.4	3.54 ± 0.3	3.52 ± 0.1
800/10	G60A40	161.32 ± 9.1	53.10 ± 1.1	1.33 ± 0.2	5.99 ± 0.3	2.55 ± 0.3	5.44 ± 0.2
	G70A30	100.82 ± 10	48.97 ± 1.8	1.34 ± 0.1	6.42 ± 0.4	2.69 ± 0.2	4.53 ± 0.2
	G80A20	58.58 ± 6.2	37.00 ± 2.2	1.54 ± 0.3	8.02 ± 0.2	5.43 ± 0.1	3.48 ± 0.1
815/05	G60A40	88.10 ± 7.1	54.11 ± 1.5	1.28 ± 0.3	6.3 ± 0.3	2.71 ± 0.3	5.44 ± 0.2
	G70A30	68.82 ± 6.7	50.18 ± 1.7	1.40 ± 0.2	6.91 ± 0.3	2.73 ± 0.2	4.49 ± 0.2
	G80A20	45.75 ± 6.0	47.65 ± 1.9	1.41 ± 0.1	7.26 ± 0.5	3.02 ± 0.1	3.40 ± 0.1
815/10	G60A40	64.54 ± 7.0	51.49 ± 2.1	1.41 ± 0.2	7.05 ± 0.3	3.58 ± 0.15	5.92 ± 0.3
	G70A30	28.13 ± 4.3	46.32 ± 1.6	1.44 ± 0.1	7.58 ± 0.2	4.94 ± 0.21	4.81 ± 0.3
	G80A20	22.21 ± 3.0	29.91 ± 1.5	1.75 ± 0.3	9.58 ± 0.2	7.93 ± 0.27	3.76 ± 0.2

through a thin liquid film to the off-contact neck region in final state sintering. This process results in a continuous reduction in pore size and a continuous change in grain shape that should become increasingly anhedral until the pore is completely eliminated. The contact flattening theory contains some inherent problems, such as the continuous reduction in pore size as the sintering time increases (from 5 to 10 min). Thus, the maximum pore size and the frequency of large pores in the pore size distribution should decrease continuously as the sintering time increases. However, this change in the pore size distribution has not been observed in real sintering experiments. Instead, the frequency of small pores decreased and that of large pores remained constant until final densification was achieved (at 800 °C and 815 °C). Another problem with the above theory

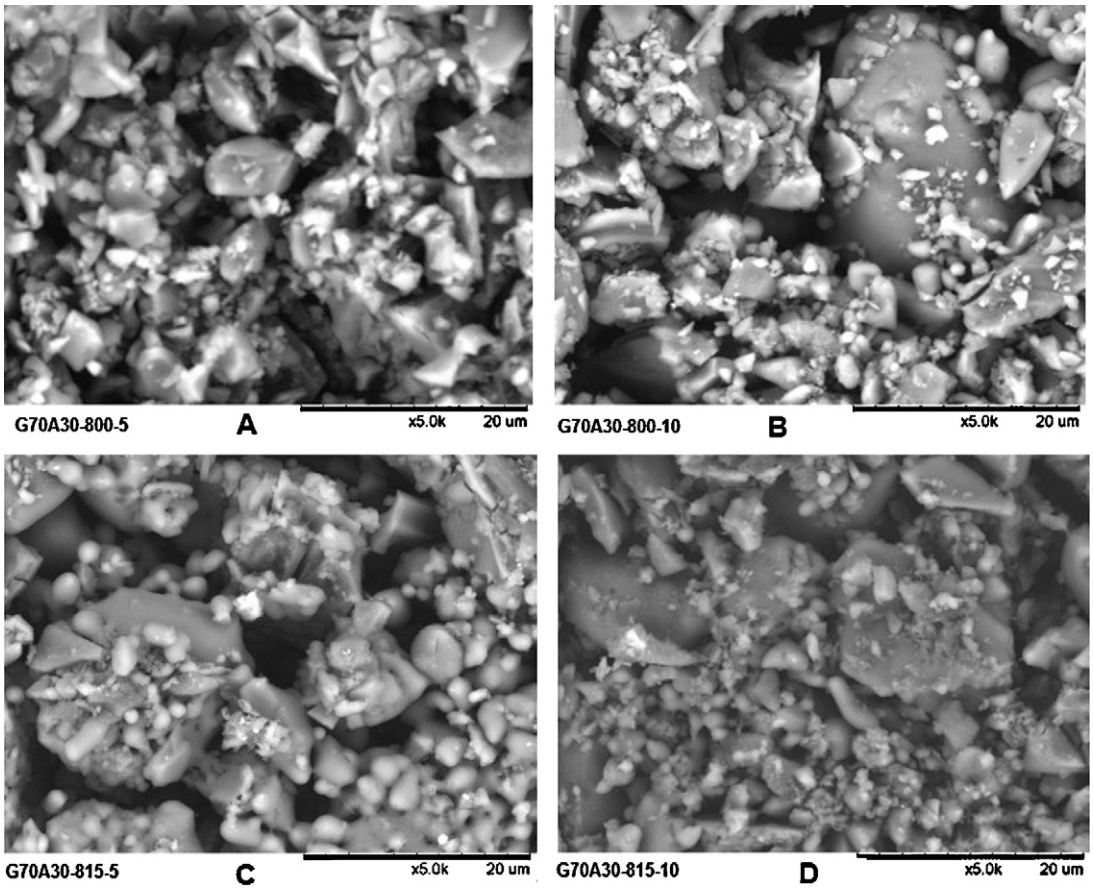

Fig. 5. SEM images of the G70A30 products sintered at 800 °C for 5 min (A), 800 °C for 10 min (B), 815 °C for 5 min (C), and 815 °C for 10 min (D).

is the proposal that a continuous change in grain shape occurs during densification. A continuous grain shape change implies that a driving force for the shape change is available as long as pores are present in the compact. In general, all of the results affirm that the final ceramics products have a mesoporous structure that has the ability to absorb and desorb environmental humidity [15].

3.2.2. Moisture adsorption–desorption properties

The moisture isotherms of the final ceramics products are shown in Fig. 6. On the basis of the IUPAC classification system [15], the shapes of the moisture isotherms belong to the Type IV class. Type IV isotherms usually possess a hysteresis loop, in which the lower and upper branches are adsorption and desorption behavior, respectively [30]. In the initial part of the isotherm (from 0% to 11% relative humidity, RH), the adsorption process is restricted to the outside of the ceramics. When the relative humidity rises to 55%, capillary condensation commences within the finest pores. At 95–100% relative humidity, the empty pores are filled with water, and the ceramics reach a saturated state. Conversely, the decrease in the amount of adsorbed water from 90% to 40% relative humidity in the desorption isotherms was attributed to the evaporation of water from the mesopores. This behavior suggests that the value for relative humidity at which the capillary condensation and evaporation processes occur are related to the size of the capillaries in porous materials by the Kelvin equation [31]. Using the Kelvin equation, the pore diameters in a ceramics material that will cause capillary condensation to occur at 55% and 95% relative humidity were calculated to be 3.5 and 40.8 nm, respectively. A comparison of these calculated values the pore sizes obtained from the pore size distribution analysis (7–10 nm) shows that capillary condensation can occur in most of the pores in these porous ceramics, according to the definition provided by Gregg and Sing [15]. However, the moisture adsorption ability of these samples was dependent of the ratio of the initial materials and their properties. This ability increases as the specific surface area, porosity, and allophane content of the samples increase. Because the absorption values increase as the capillary upswing of the isotherm moves to larger relative pressures and becomes steeper, the hysteresis loops become more pronounced as the ability of the ceramic to control the humidity increases [32]. On the basis of these results, the incorporation of allophane in silica-based materials

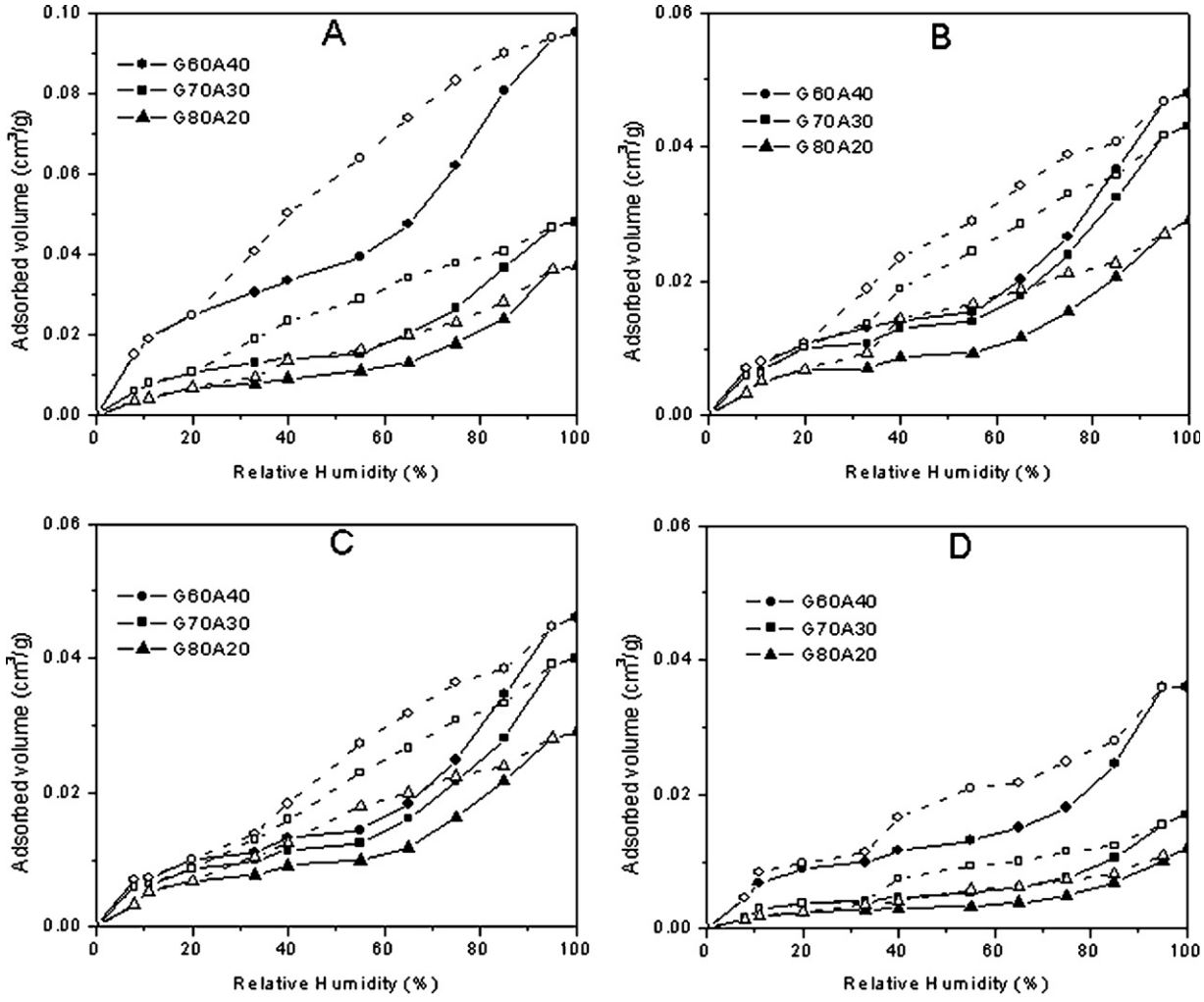

Fig. 6. Water adsorption - desorption isotherms of the final ceramic products sintered at 800 °C for 5 min (A), 800 °C for 10 min (B), 815 °C for 5 min (C), and 815 °C for 10 min (D). *(Solid lines: adsorption; dashed lines: desorption).*

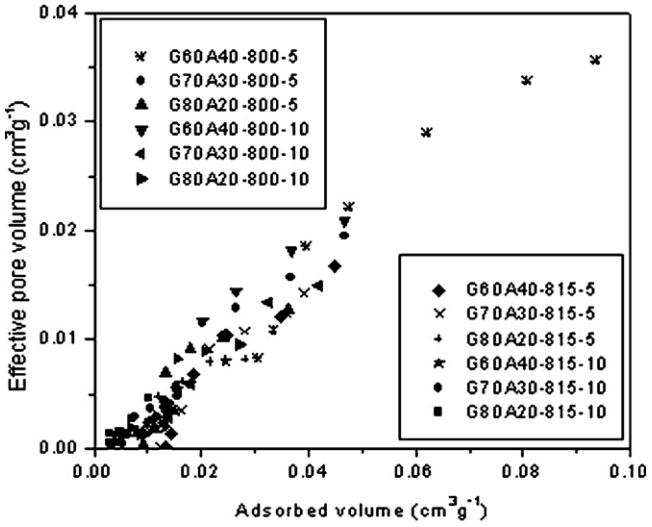

Fig. 7. Equilibrium adsorption ability of the products. (*G60A40-800-5 is the G60A40 sample sintered at 800 °C for 5 min*).

increased the moisture adsorption ability of the final porous ceramics.

3.2.3. Equilibrium adsorption ability

The equilibrium adsorption abilities of the ceramic products are shown in Fig. 7. Effective pore volumes (vertical axis) were calculated using the BET method with multiform pore shapes. The adsorbed volumes (horizontal axis) were measured from the moisture isotherms. The relationship between the two volume values is derived using the Kelvin equation on the basis of pore diameter. The equilibrium adsorption ability of each sample was determined for seven RH values, including 33, 40, 55, 65, 75, 85 and 95%. Because the occurrence of capillary condensation is intimately connected to the curvature of a liquid meniscus, there are geometric constraints on cluster formation with monolayer adsorption at small RH values, and the difference between the effective pore volume and the adsorbed volume is slight. These findings further support the proposal of Do and Do [33]. Thus, RH increased, and the adsorbed moisture continuously increased through the ''multi-layer'' region until the diversified pore system was filled via capillary condensation, the definition of which is presented by Gregg and Sing [15]. All of the samples exhibited a trend in which the adsorbed volume was higher than the effective pore volume because the effective pore volumes determined from the BET results included micropores and mesopores. The moisture first diffused from the environment into the micropore, then the mesopore, and then part of the macropore or larger pore. Thus, the adsorbed volume of moisture is always larger than the effective volume at the equilibrium state. These results are consistent with those of other studies [13,16] and suggest that the final ceramic products ability to control humidity stems from the capillary condensation mechanism.

3.2.4. Other mechanical properties

Some additional mechanical properties of final products are shown in Table 3. The results showed that the bending strengths of all of the porous ceramics are higher than 6 MPa, except for those generated at 800 °C for 5 min, with 60% waste glass and 40% weathered volcanic ash. These values satisfy the Japanese Industrial Standard (JIS) for the bending strength test. When the waste glass contents, sintering temperature and holding time increase, the values of bending strength also increases; the ignition loss decreases as the waste glass content in the products increases. However, the effects of sintering temperature and holding time on ignition loss and bulk density are slight. Some researchers have described the influence of particle size homogeneity on the kinetics of sintering. Zhao and Harmer [34,35] theoretically and experimentally analyzed the influence of the particle size distribution and homogeneity on the sintering kinetics. They found that particle size homogeneity leads to a decrease in grain growth and to a subsequent increase in the sintering rate and decrease in the densification. In addition, Patterson and co-authors [36,37] have experimentally shown that the particle size distribution and homogeneity influence the integral shrinkage. Here, an increase in the sintering rate is a characteristic for large particles if the particle size inhomogeneity increases. The non-monotonous dependence of the densification on various particle sizes with a minimum in the intermediate region is a characteristic for small particles. In this study, the results in Fig. 2 show that 75 wt% of the waste glass particles are homogenous and ranges in size

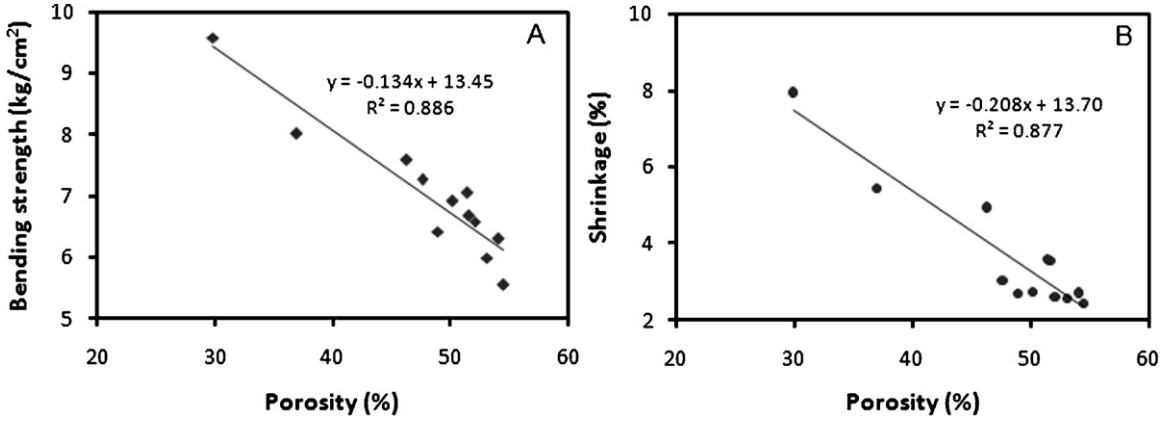

Fig. 8. Relationship between the porosity and mechanical characteristics: (A) Bending strength and (B) shrinkage.

Table 4
TCLP leaching concentrations of heavy metals in the raw materials and the final products (mg/l).

Sintering temp./time (°C/min)	Sample	Pb	Cd	Cr	Cu	Zn
800/05	G60A40	0.18	N.D.	N.D.	0.3	0.26
	G70A30	0.21	N.D.	N.D.	0.19	0.25
	G80A20	0.27	N.D.	N.D.	0.16	0.27
800/10	G60A40	0.19	N.D.	N.D.	0.29	0.25
	G70A30	0.2	N.D.	N.D.	0.2	0.25
	G80A20	0.25	N.D.	N.D.	0.14	0.27
815/05	G60A40	0.17	N.D.	N.D.	0.31	0.26
	G70A30	0.2	N.D.	N.D.	0.21	0.26
	G80A20	0.26	N.D.	N.D.	0.13	0.24
815/10	G60A40	0.18	N.D.	N.D.	0.28	0.25
	G70A30	0.2	N.D.	N.D.	0.2	0.25
	G80A20	0.26	N.D.	N.D.	0.15	0.26
Waste glass	0.31	N.D.	N.D.	N.D.	0.26	
Volcanic ash	N.D.	N.D.	N.D.	0.7	0.27	
Regulatory (US EPA)	5	1	5	15	-	

N.D.: Values are below equipment detection limit (Zn: 0.005 ppm, Pb: 0.009 ppm, Cu: 0.005 ppm, Cr: 0.006 ppm, Cd: 0.008 ppm). US EPA: United States Environmental Protection Agency.

from 9 to 25 μm. However, 20 wt% of the waste glass particles are quite fine and are less than 9 μm in size. This fineness is linked to inhomogeneities in the waste glass and is a factor that affects the physical properties of final ceramic products. Thus, the waste glass contents in the samples increase as the glass fineness ratio increases, and the density, bending strength and shrinkage values of the porous ceramics also increase. Furthermore, according to sintering theory [29], the density, bending strength and shrinkage values increase as the porosity decreases. The relationship between the porosity and the mechanical characteristics of the porous ceramic can be studied by identifying the values that limit the measured porosity, if any, to substitute for the specific weight absorption and hardness requirements [38]. The results of these studies are shown in Fig. 8, including the relationship between the porosity and bending strength with regression coefficient of $R^2 = 0.89$ (Fig. 8A). As expected, the porosity decreases as the bending strength increases. The relationship between the porosity and the shrinkage of the porous ceramics used in this study is also shown in Fig. 8B. A linear relationship with $R^2 = 0.88$ can be observed with data points scattered near the region of higher porosity. In general, all of the mechanical properties affirm that all of the final ceramics products satisfied the standards for commercial ceramics.

The leaching concentrations of heavy metals, which are based on the TCLP test, are shown in Table 4. The results indicate that leaching concentrations of Pb increase and those of Cu decrease as the waste glass component in the final ceramic products increases. However, the leaching concentration of Zn changes only slightly for almost all products. In general, the leaching concentrations of heavy metals in the final products are all well below the regulatory limits of the US EPA, indicating that the final products are safe if used as construction materials.

The selection of the best ceramic product should satisfy two basic conditions: high water adsorption ability and good mechanical characteristics that meet or exceed the necessary standards, especially bending strength values. Therefore, on the basis of all the observed features of these ceramic products, the G70A30 sample sintered at 800 °C for 5 min is clearly the most superior ceramic product.

4. Conclusion

This study investigated the feasibility of generating humidity-control porous ceramics by sintering a mixture of volcanic ash and waste glass. The sintering conditions, including sintering time, sintering temperature, and various ratios of the initial materials, were tested. The final products were analyzed to identify the moisture isotherms, the equilibrium moisture contents, and the porous and mechanical properties.

The results showed that the adsorption–desorption moisture capacities and mechanical properties of the final products are significantly effected by the amount of weathered volcanic ash in the ratio of raw materials and the sintering conditions (sintering temperature and holding time). The porous ceramics produced in this study exhibit excellent performance as a humidity-controlling building material with adjustable properties, and they could be used for building applications in the near future. The TCLP leaching concentrations of heavy metals in the final products are lower than those prescribed by regulations.

The experimental conditions for manufacturing porous ceramics that exhibit the best properties are: 30% weathered volcanic ash, 70% waste glass, a sintering temperature of 800 °C and holding time of 5 min. The properties of this ceramic product include a BET surface area of 163.73 ± 12 m^2/g, 52.08 ± 2.1% porosity, and a pore size of approximately 9 nm in diameter. The total amount of adsorbed water was 0.047 cm^3/g. Furthermore, the mechanical characteristics are also appropriate for use as a commercial porous ceramic with a bulk density of 1.34 ± 0.2 g/cm^3, 2.61 ± 0.1% shrinkage, 4.64 ± 0.3% ignition loss, and 6.58 ± 0.4 MPa bending strength.

Acknowledgements

This work was financially supported in part by the Waste Management and Resource Recovery Group, Graduate Institute of Environmental Engineering, National Central University, Jhongli, Taoyuan 32001, Taiwan.

References

[1] Y. Tomita, R. Takahashi, S. Sato, T. Sodesawa, M. Otsuta, Humidty control ability of silica with bimodal pore structures prepared from water glass, J. Ceram. Soc. Jpn. 112 (2004) 491–495.
[2] T. Horikawa, Y. Kitakaze, T. Sekida, T. Sekida, M. Katoh, Characteristics and humidity control capacity of activated carbon from bamboo, Bioresour. Technol. 101 (2010) 3964–3969.
[3] T. Zimny, G. Finqueneisel, L. Cossarutto, J.V. Weber, Water vapor adsorption on activated carbon preadsorbed with naphtalene, J. Colloid Interface Sci. 285 (2005) 56–60.
[4] K.B. Adhikary, S. Pang, M.P. Staiger, Long-term moisture absorption and thickness swelling behaviour of recycled thermoplastics reinforced with Pinus radiata sawdust, Chem. Eng. J. 142 (2008) 190–198.
[5] V. Vendange, Ph. Colomban, F. Larch, Pore size and liquid impregnation of microporous aluminosilicate, Micro. Mater. 5 (1996) 389–400.
[6] J.C. Gonzalez, M. Molina-Sabio, F. Rodríguez-Reinoso, Sepiolite-based adsorbents as humidity controller, Appl. Clay Sci. 20 (2001) 111–118.
[7] T. Nakazato, F. Yano, K. Ohyama, T. Uchibori, N. Nakagawa, Moisture absorption characteristics of porous calcium oxide powders produced by calcination of pulveriezed limestone with inorganic salts using a powder-particle fluidized bed, J. Ceram. Soc. Jpn. 115 (2007) 443–446.
[8] S. Fukushima, Y. Inagaki, Adsorption of water vapor and hydrophobicity of ordered mesoporous silica, FSM-16, Micro. Meso. Mater. 21 (1998) 667–672.
[9] T. Kanno, K. Kawamura, K. Toda, J. Horiuchi, M. Kobayashi, Effect of humidity on adsorption behavior of acetaldehyde on a diatomaceous material, J. Ceram. Soc. Jpn. 111 (2003) 396–400.
[10] Farid Akhtar, Petr O. Vasiliev, Lennart Bergstrom, Hierarchically porous ceramics from diatomite powders by pulsel curent processing, J. Am. Ceram. Soc. 92 (2009) 338–343.
[11] F. Caturla, M. Molina-Sabio, F. Rodriguez-Reinoso, Adsorption–desorption of water vapor by natural and heat-treated sepiolite in ambient air, Appl. Clay Sci. 15 (1999) 367–380.
[12] T. Kimura, M. Suzuki, M. Maeda, S. Tomura, Water adsorption behavior of ordered mesoporous silicas modified with an organosilane composed of hydrophobic alkyl chain and hydrophilic polyethylene oxide groups, Micro. Meso. Mater. 95 (2006) 213–219.
[13] F. Hiroshi, Y. Shigeru, K. Kazuko, Study on a New Humidity Controlling Material Porous Soil "Allophane"-Design of Humidity Controlling Material, Resour. Process. 52 (2005) 128–135.
[14] M. Maeda, M. Suzuki, F. Ohashi, K. Inukai, S. Tomura, Y. Shibasaki, K. Aikawa, K. Okada, Water vapor adsorption of porous materials of AlOOH–Al_2O_3, J. Ceram. Soc. Jpn. 110 (2002) 118–120.
[15] Gregg S.J., Sing K.S.W. Adsorption, Surface Area and Porosity (2ed). s.l.: AP; 1982.
[16] Dinh-Hieu Vu, Kuen-Sheng Wang, Bui Hoang Bac, Humidity control porous ceramics prepared from waste and porous materials, Mater. Lett. 65 (2011) 940–943.
[17] Emmanuelle Montarges-Pelletier, Sandrine Bogenez, Manuel Pelletier, Angelina Razafitianamaharavo, Jaafar Ghanbaja, Bruno Lartiges, Laurent Michot, Synthetic allophane-like particles: textural properties, Collo. Surf. A 255 (2005) 1–10.
[18] H. Maeda, Emile H. Ishida, Water vapor adsorption and desorption of mesoporous materials derived from metakaolinite by hydrothermal treatment, Ceram. Int. 35 (2008) 987–990.
[19] Gottlieb.-G. Lindner, Hiromoto Nakazawa, Shigenobu Hayashi, Hollow nanospheres, allophanes 'All-organic' synthesis and characterization, Micro. Meso. Mater. 21 (1998) 381–386.
[20] Thierry Woignier, G. Pochet, H. Doumenc, P. Dieudonńe, L. Duffours, Allophane: a natural gel in volcanic soils with interesting environmental properties, J Sol–Gel Sci. Technol. 41 (2007) 25–30.
[21] Thierry Woignier, Juan Primera, Laurent Duffours, Philippe Dieudonné, Abdelazize Raada, Preservation of the allophanic soils structure by supercritical drying, Micro. Meso. Mater. 190 (2008) 370–375.
[22] Einstine Opiso, Tsutomu Sato, Tetsuro Yoneda, Adsorption and co-precipitation behavior of arsenate, chromate, selenate and boric acid with synthetic allophane-like materials, J. Haza. Mater. 170 (2009) 79–86.
[23] ASTM C1498-01. Standard Test Method for Hygroscopic Sorption Isotherms of Building Materials.
[24] ASTM C1674-08 Standard Test Method for Flexural Strength of Advanced Ceramics with Engineered Porosity (Honeycomb Cellular Channels) at Ambient Temperatures.
[25] ASTM D7348-08 Standard Test Methods for Loss on Ignition (LOI) of Solid Combustion Residues.
[26] ASTM C20-00(2010) Standard Test Methods for Apparent Porosity, Water Absorption, Apparent Specific Gravity, and Bulk Density of Burned Refractory Brick and Shapes by Boiling Water.
[27] A. Das, N. Das, M.K. Naskar, D. Kundu, M. Chatterjee, H.S. Maiti, Influence of process parameters on the formation of Silicalite-1 zeolite particles, Ceram. Int. 35 (2009) 1799–1806.
[28] D.U. Tulyaganov, M.J. Ribeiro, J.A. Labrincha, Development of glass-ceramics by sintering and crystallization of fine powders of calcium-magnesium-aluminosilicate glass, Ceram. Int. 28 (2002) 515–520.
[29] L.K. Suk-Joong, Sintering - Densification, Grain Growth, and Microstructure, Elsevier Butterworth-Heinemann, Oxford, UK, 2005.
[30] M. El-Sabaawi, D.C.T. Pei, Moisture isotherms of hygroscopic porous solids, Ind. Eng. Chem. Fundamen. 16 (1977) 321–326.
[31] Kiyoshi Okada, Yoshitoshi Saito, Masanori Hiroki, Takahiro Tomita, Water vapor sorption on mesoporous gamma-alumina prepared by the selective leaching method, J. Porous. Mater. 4 (1997) 253–260.
[32] I.A. Rahman, P. Vejayakumaran, C.S. Sipaut, J. Ismail, C.K. Chee, Effect of the drying techniques on the morphology of silica nanoparticles synthesized via sol–gel process, Ceram. Int. 34 (2008) 2059–2066.
[33] D.D. Do, H.D. Do, A model for water adsorption in activated carbon, Carbon 38 (2000) 767–773.
[34] Junhong Zhao, Martin P. Harmer, Effect of pore distribution on microstructure development: I. Matrix pores, J. Am. Ceram. Soc. 71 (1988) 113–120.
[35] Junhong Zhao, Martin P. Harmer, Effect of pore distribution on microstructure development: II. First and second generations, J. Am. Ceram. Soc. 71 (1988) 530–539.
[36] B.R. Patterson, L.A. Benson, The effect of powder size distribution on sintering, Prog. Powd. Metall. 39 (1983) 215–230.
[37] B.R. Patterson, J.A. Griffin, Effect of particle size distribution on sintering of tungsten, Mod. Dev. Powd. Metall 15 (1984) 279–288.
[38] Kae-Long. Lin, Use of thin film transistor liquid crystal display (TFT-LCD) waste glass in the production of ceramic tiles, J. Haza. Mater. 148 (2007) 91–97.